References

AUTHIER, A. & SIMON, D. (1968). *Acta Cryst.* A**24**, 517-526.
BORN, M. & WOLF, E. (1965). *Principles of Optics.* Oxford: Pergamon.
TAKAGI, S. (1962). *Acta Cryst.* **15**, 1311-1312.
TAKAGI, S. (1969). *J. Phys. Soc. Jpn*, **26**, 1239-1253.
TAUPIN, D. (1964). *Bull. Soc. Fr. Minéral. Cristallogr.* **87**, 469-511.
URAGAMI, T. (1969). *J. Phys. Soc. Jpn*, **27**, 147-154.

Acta Cryst. (1987). A**43**, 525-533

Investigation of Short-Range Order in Ni–10 at.% Al Single Crystals by Diffuse X-ray Scattering

BY F. KLAIBER, B. SCHÖNFELD AND G. KOSTORZ

Institut für Angewandte Physik, Eidgenössische Technische Hochschule Zürich, ETH-Hönggerberg, CH-8093 Zürich, Switzerland

(*Received* 15 *September* 1986; *accepted* 13 *January* 1987)

Abstract

The diffuse scattering from single crystals of nominally Ni-10 at.% Al, quenched after heat treatment at 973 K, has been measured with Mo $K\alpha$ radiation. The data were analysed for the contributions due to short-range order and static atomic displacements. Consistency of the structural parameters as determined by three different methods, the separation methods of Georgopoulos-Cohen and Borie-Sparks and the least-squares method of Williams, is demonstrated for the first time. The variation of the first few short-range-order parameters α_{lmn} with the coordination shell *lmn* strongly resembles that of the $L1_2$ superstructure. Employing these parameters to model a short-range-ordered computer crystal with 13 104 atoms, a preference for configurations of the $L1_2$ superstructure type is found, though no Ni_3Al embryos are observed. The values of α_{lmn} rapidly reach those for a random solid solution.

1. Introduction

Nickel base superalloys are technologically important because of their favourable mechanical properties at temperatures up to about 1200 K. In many of these alloys, ordered Ni_3Al-type precipitates (γ' phase with $L1_2$ superstructure), coherent with the γ matrix, are responsible for high mechanical strength by impeding dislocation motion. Ni-Al solid solutions may be seen as a prototype of other superalloys that can be obtained by a partial substitution of the Ni and Al atoms.

Ordering and decomposition have been studied in Ni-Al alloys as well as in technological alloys by various methods, such as small-angle neutron scattering (Beddoe, Haasen & Kostorz, 1984), transmission electron microscopy (Gröhlich, Haasen & Frommeyer, 1982) and atom-probe field-ion microscopy (Wendt & Haasen, 1983). Earlier work is found in the references just quoted.

High-angle scattering has been employed to study local atomic arrangements in various binary Ni-rich alloys, such as Ni-Cr, Ni-Mo, Ni-Fe; for a review see Kostorz (1983). One high-angle scattering measurement on Ni-12·7 at.% Al was recently performed by Epperson & Fürnrohr (1983). The short-range-ordered state quenched in from 1323 K was analysed by the method introduced by Borie & Sparks (1971).

In the present study, single crystals of Ni with nominally 10 at.% Al were used for an investigation of short-range order. As this concentration is still within the γ region, the formation of γ' particles is avoided, and the short-range-ordering properties of the γ phase may be investigated. The method of Georgopoulos & Cohen (1977), most appropriate for the diffuse scattering of X-rays, is employed to analyse the data. This method also allows individual atomic displacements to be determined. Two other methods, the one proposed by Borie & Sparks (1971) and the least-squares method suggested by Williams (1972), have also been applied in order to evaluate the influence of various methods on the resulting structural parameters.

2. Experimental

A single crystal of Ni with nominally 10 at.% Al, about 6 cm long and 12 mm in diameter, was grown under an argon (5N7) atmosphere in a high-purity Al_2O_3 crucible by the Bridgman technique; the starting alloy was prepared from 99·99 at.% Ni and 99·999 at.% Al. The single crystal was homogenized in argon for 24 h at 1373 K and water quenched. Subsequently two slices about 3 mm thick, with a surface normal near the [119] direction, were spark

0108-7673/87/040525-09$01.50

cut. The chemical analysis of the two samples yielded an Al concentration of 9·5 and 9·8 at.%, respectively. Both samples were heat treated at 973 K, sample 1 (with 9·5 at.% Al) for 48 h and sample 2 (with 9·8 at.% Al) for 3354 h, and water quenched. To remove any surface damage, the samples were polished mechanically and electrochemically. The final samples showed a typical mosaicity of 0·7° full width at half maximum.

Diffuse X-ray measurements were carried out on a four-circle diffractometer at room temperature in symmetrical reflection geometry. A sealed Mo tube operated at 44 mA and 50 kV was used as X-ray source. The Mo $K\alpha$ radiation (wavelength $\lambda =$ 0·71069 Å) was selected by a singly bent and a doubly bent pyrolytic graphite monochromator for sample 1 and sample 2, respectively. Furthermore, the beam divergences were adjusted by slits to allow measurements of the diffuse intensity to be taken at points separated by 0·1 reciprocal-lattice units. To eliminate effects due to instabilities of the X-ray source, the incident-beam intensity was normalized to the scattered radiation from a thin Mylar foil, mounted just in front of the sample. A fixed point on the sharp tail of a Bragg reflection was also measured about every 2 h to indicate any mechanical/electronic instability of the set-up. An ORTEC high-purity Ge detector with an energy resolution of better than 400 eV for Mo $K\alpha$ was used to measure the diffuse intensity from the sample. Thus, the intensity contributions due to fluorescence scattering and the $\lambda/2$ harmonic could be eliminated by a pulse-height analyser. Care was taken to include the Compton-scattering contributions for all scattering angles used. Whereas for sample 1 the total X-ray path was in air at atmospheric pressure, sample 2 was mounted in an evacuated sample chamber covered by a thin Be hemisphere. In this case the background, mainly due to air scattering, was distinctly reduced.

The diffuse intensity was measured for each sample at about 8000 positions in reciprocal space, with the scattering angle 2θ ranging from 18 to 90°. Typical counts were $1{\cdot}7\times10^3$ to $1{\cdot}2\times10^4$ in about 330 s.

After correcting the measured intensities for background, surface roughness, absorption by the Be hemisphere and partial passing of the beam at the sample, absolute intensities were calculated. For calibration, two methods were used (see Schwartz & Cohen, 1977): firstly, the integrated intensities of the 111, 200 and 220 Bragg reflections of an Al-powder compact (Batterman, Chipman & de Marco, 1961) and, secondly, the scattering of polystyrene at $\sin\theta/\lambda = 0{\cdot}5$ Å^{-1} (Sparks & Borie, 1965) were measured. The conversion factors of these two independent methods agreed within 5%. The polarization factor K of the incident beam was found experimentally (see *e.g.* Le Page, Gabe & Calvert, 1979) to be $K = 0{\cdot}988\,(7)$ and $0{\cdot}978\,(3)$ for sample 1 and sample 2, respectively. The Compton scattering was subtracted using the data of Cromer (1969). Thermal diffuse scattering up to third order (TDS_1, TDS_2 and TDS_3) was calculated, using the nearest-neighbour force constants (Warren, 1969) as obtained from the elastic constants of Pottebohm, Neite & Nembach (1983). An overall thermal Debye-Waller factor (DWF) of $\exp[-2B(\sin\theta/\lambda)^2]$ was determined by measuring integrated intensities of various Bragg reflections; $B = 0{\cdot}315\,(13)$ Å^2 was obtained for both samples. Finally, the atomic scattering factors of Ni and Al were taken from Doyle & Turner (1968) and the dispersion corrections from Cromer & Liberman (1970).

3. Theory

The diffuse X-ray scattering from a binary (A-B) cubic single crystal has been discussed in various papers (Borie & Sparks, 1971; Georgopoulos & Cohen, 1977; Williams, 1972). Here we summarize the results starting from the presentation of Georgopoulos & Cohen (1977). In their formulation, the total diffuse intensity $I_D(\mathbf{k})$, where $\mathbf{k}$ is the scattering vector ($k = 4\pi\sin\theta/\lambda$), - expanding the static atomic displacements up to quadratic terms and the thermal diffuse scattering up to third order - is given by

$$\begin{aligned}
I_D(\mathbf{k}) = {} & \mathrm{TDS}_2(\mathbf{k}) + \mathrm{TDS}_3(\mathbf{k}) \\
& + Nc_A c_B |f'_A - f'_B|^2 \{ I_{\mathrm{SRO}}(\mathbf{k}) \\
& + h_1[\eta Q_x^{AA}(\mathbf{k}) + \xi Q_x^{BB}(\mathbf{k})] \\
& + h_2[\eta Q_y^{AA}(\mathbf{k}) + \xi Q_y^{BB}(\mathbf{k})] \\
& + h_3[\eta Q_z^{AA}(\mathbf{k}) + \xi Q_z^{BB}(\mathbf{k})] \\
& + h_1^2[\tilde{\eta}^2 R_x^{AA}(\mathbf{k}) + 2\tilde{\eta}\tilde{\xi} R_x^{AB}(\mathbf{k}) + \tilde{\xi}^2 R_x^{BB}(\mathbf{k})] \\
& + h_2^2[\tilde{\eta}^2 R_y^{AA}(\mathbf{k}) + 2\tilde{\eta}\tilde{\xi} R_y^{AB}(\mathbf{k}) + \tilde{\xi}^2 R_y^{BB}(\mathbf{k})] \\
& + h_3^2[\tilde{\eta}^2 R_z^{AA}(\mathbf{k}) + 2\tilde{\eta}\tilde{\xi} R_z^{AB}(\mathbf{k}) + \tilde{\xi}^2 R_z^{BB}(\mathbf{k})] \\
& + h_1 h_2[\tilde{\eta}^2 S_{xy}^{AA}(\mathbf{k}) + 2\tilde{\eta}\tilde{\xi} S_{xy}^{AB}(\mathbf{k}) + \tilde{\xi}^2 S_{xy}^{BB}(\mathbf{k})] \\
& + h_1 h_3[\tilde{\eta}^2 S_{xz}^{AA}(\mathbf{k}) + 2\tilde{\eta}\tilde{\xi} S_{xz}^{AB}(\mathbf{k}) + \tilde{\xi}^2 S_{xz}^{BB}(\mathbf{k})] \\
& + h_2 h_3[\tilde{\eta}^2 S_{yz}^{AA}(\mathbf{k}) + 2\tilde{\eta}\tilde{\xi} S_{yz}^{AB}(\mathbf{k}) + \tilde{\xi}^2 S_{yz}^{BB}(\mathbf{k})]\},
\end{aligned} \tag{1}$$

where N is the number of atoms in the beam, f'_A and f'_B are the atomic scattering factors (including an overall Debye-Waller factor) and c_A and c_B are the atomic fractions of the components. Interatomic vectors $\mathbf{r}$ are expressed by

$$\mathbf{r} = l(\mathbf{a}_1/2) + m(\mathbf{a}_2/2) + n(\mathbf{a}_3/2), \tag{2}$$

where $\mathbf{a}_i$ are the translation vectors of the cubic unit cell and l, m, n are integers defining a particular lattice

site. As the scattering-factor ratios

$$\eta = \mathrm{Re}\,[f'_A/(f'_A - f'_B)], \quad \xi = \mathrm{Re}\,[f'_B/(f'_A - f'_B)],$$
$$\widetilde{\eta\xi} = \mathrm{Re}\,(f'_A f'^{*}_B)/|f'_A - f'_B|^2,$$
$$\tilde{\eta}^2 = |f'_A|^2/|f'_A - f'_B|^2 \quad \text{and} \quad \tilde{\xi}^2 = |f'_B|^2/|f'_A - f'_B|^2 \quad (3)$$

vary as a function of $\mathbf{k}$, the 25 intensity components [$I_{\mathrm{SRO}}(\mathbf{k})$, $Q_x^{AA}(\mathbf{k})$, $Q_x^{BB}(\mathbf{k})$ *etc.*], which are all strictly periodic functions in reciprocal space, can be separated from one another. The Fourier coefficients α_{lmn} of the short-range-order series

$$I_{\mathrm{SRO}}(\mathbf{k}) = \sum_l \sum_m \sum_n \alpha_{lmn} \cos \pi h_1 l \cos \pi h_2 m \cos \pi h_3 n \quad (4)$$

are the Warren–Cowley short-range-order parameters (Cowley, 1950):

$$\alpha_{lmn} = 1 - P^{AB}_{lmn}/c_B, \quad (5)$$

where P^{AB}_{lmn} is the probability of finding a B-type atom at site lmn, if an A-type atom is at site 000, and h_i are the Miller indices of the reciprocal-lattice point considered [$\mathbf{k} = 2\pi(h_1, h_2, h_3)/a$, lattice parameter a].

The Q series in (1) describe the intensities due to first-order static displacements. They may be written as

$$Q_x^{AA}(\mathbf{k}) = -2\pi \sum_l \sum_m \sum_n (c_A/c_B + \alpha_{lmn}) \times \langle x^{AA}_{lmn} \rangle \sin \pi h_1 l \cos \pi h_2 m \cos \pi h_3 n, \quad (6)$$

with similar expressions for the other first-order terms. The Fourier coefficients $\langle x^{AA}_{lmn} \rangle$ describe the average static displacements from the average lattice in the x direction of an A-type atom near a site lmn if an A-type is at site 000.

The R and S series in (1) contain Fourier coefficients that are bilinear in the atomic displacements. The corresponding terms may be written as

$$R_x^{AA}(\mathbf{k}) = -2\pi^2 \sum_l \sum_m \sum_n (c_A/c_B + \alpha_{lmn}) \times \langle (\tilde{x}^{AA}_{lmn})^2 \rangle \cos \pi h_1 l \cos \pi h_2 m \cos \pi h_3 n \quad (7)$$

$$S_{xy}^{AA}(\mathbf{k}) = 4\pi^2 \sum_l \sum_m \sum_n (c_A/c_B + \alpha_{lmn}) \times \langle (\tilde{x}^{AA}_{lmn})(\tilde{y}^{AA}_{lmn}) \rangle \sin \pi h_1 l \sin \pi h_2 m \cos \pi h_3 n$$

where, for example, $\langle (\tilde{x}^{AA}_{000})(\tilde{y}^{AA}_{lmn}) \rangle$ describes the correlations of static and dynamic displacements, if there is an A atom at site lmn and another A atom at site 000.

If the intensities at 50 to 60 symmetrically related positions in reciprocal space are known for each point of $I_{\mathrm{SRO}}(\mathbf{k})$ within its minimum separation volume (see *e.g.* Matsubara & Cohen, 1983), the various intensity components can be obtained everywhere in reciprocal space. A Fourier inversion of these terms then leads to the structural parameters (*e.g.* α_{lmn}). If one assumes that the scattering-factor ratios of (3) do not vary with the scattering vector $\mathbf{k}$, one can incorporate them in the various series, thus reducing the number of unknown functions to ten. This formulation corresponds to that of Borie & Sparks (1971). The first-order displacement coefficients γ^x_{lmn} are now given by

$$\gamma^x_{lmn} = -2\pi[\eta(c_A/c_B + \alpha_{lmn}) \times \langle x^{AA}_{lmn} \rangle - \xi(c_B/c_A + \alpha_{lmn}) \langle x^{BB}_{lmn} \rangle]. \quad (8)$$

With this separation scheme the intensity components must be separated by least-squares fitting (Wu, Matsubara & Cohen, 1983) and not a combinatorial procedure as proposed by Gragg & Cohen (1971). Finally, if one expands the series in the Borie–Sparks formulation up to a certain number of significant Fourier coefficients, the structural parameters (α_{lmn}, γ^x_{lmn} *etc.*) are directly obtained by a least-squares fitting of these parameters to the data. This was first demonstrated by Williams (1972).

4. Results

For a data analysis according to Georgopoulos & Cohen (1977), points in reciprocal space are chosen according to symmetry considerations. Thus they will not in general cover a contiguous range in $\mathbf{k}$ space. For an easy visualization of the modulation of the diffuse intensity and the various contributions to it, Fig. 1 shows the diffuse intensity along an [$hh0$] direction around the 330 position for sample 1. Differences between sample 1 and sample 2 are too small to be resolved in such a representation. The measured diffuse intensity (○) is plotted after subtraction of TDS_2, TDS_3 and Compton scattering (▲) and finally without TDS_1 (×), too. For comparison,

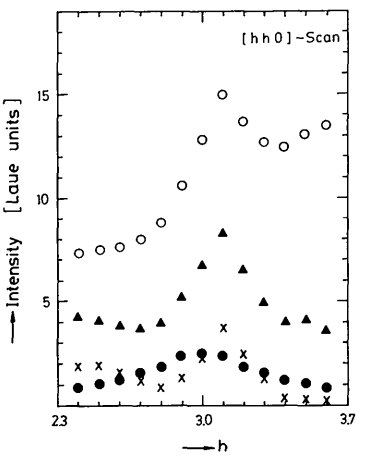

Fig. 1. Diffuse scattering intensity $I_D(\mathbf{k})$ (○) and $I_{\mathrm{SRO}}(\mathbf{k})$ (●) of sample 1 in the [$hh0$] direction close to the 330 position. Data are also given after subtraction of TDS_2, TDS_3, Compton scattering (▲) and of TDS_1 (×), too.

Table 1. *Warren–Cowley short-range-order parameters α_{lmn} for the various evaluation methods and the modelled coefficients*

Shell index *lmn*	Georgopoulos & Cohen (1977)	Borie & Sparks (1971)	Williams (1972)	Averaged experimental parameters	Modelled parameters
Sample 1					
0 0 0	1·1926 (81)	1·1866 (166)	1·2171 (43)	1·1988 (162)	1·0000
1 1 0	−0·0914 (94)	−0·0896 (45)	−0·0833 (33)	−0·0881 (43)	−0·0879 (1)
2 0 0	0·0479 (23)	0·0452 (74)	0·0560 (28)	0·0497 (56)	0·0496 (1)
2 1 1	−0·0079 (13)	−0·0063 (25)	0·0007 (22)	−0·0045 (46)	−0·0045 (1)
2 2 0	0·0339 (19)	0·0303 (55)	0·0368 (18)	0·0337 (33)	0·0337 (1)
3 1 0	−0·0132 (16)	−0·0134 (38)	−0·0071 (14)	−0·0112 (36)	−0·0113 (1)
2 2 2	0·0162 (23)	0·0118 (68)	0·0133 (12)	0·0138 (22)	0·0139 (2)
3 2 1	−0·0012 (9)	−0·0021 (25)	−0·0016 (9)	−0·0016 (5)	−0·0017 (0)
4 0 0	0·0020 (29)	0·0120 (82)	0·0069 (8)	0·0070 (50)	0·0068 (2)
3 3 0	0·0003 (19)	0·0010 (51)	−0·0019 (6)	−0·0002 (15)	−0·0002 (2)
4 1 1	0·0032 (15)	0·0041 (36)	0·0032 (5)	0·0035 (5)	0·0034 (1)
4 2 0	0·0031 (14)	0·0042 (39)	0·0044 (5)	0·0039 (7)	0·0039 (1)
3 3 2	−0·0025 (14)	−0·0052 (38)	−0·0041 (4)	−0·0039 (14)	−0·0039 (1)
4 2 2	−0·0016 (13)	0·0003 (33)	−0·0010 (4)	−0·0008 (11)	−0·0008 (1)
Sample 2					
0 0 0	1·0181 (113)	0·9899 (238)	1·1193 (481)	1·0424 (680)	1·0000
1 1 0	−0·0966 (33)	−0·0976 (66)	−0·0991 (37)	−0·0977 (13)	−0·0975 (2)
2 0 0	0·0420 (44)	0·0417 (123)	0·0577 (32)	0·0471 (92)	0·0469 (2)
2 1 1	0·0013 (17)	0·0046 (33)	0·0046 (25)	0·0035 (19)	0·0035 (1)
2 2 0	0·0265 (28)	0·0261 (92)	0·0279 (21)	0·0268 (9)	0·0268 (2)
3 1 0	−0·0102 (23)	−0·0072 (51)	−0·0030 (17)	−0·0068 (36)	−0·0069 (1)
2 2 2	0·0162 (33)	0·0093 (94)	0·0068 (25)	0·0107 (49)	0·0102 (2)
3 2 1	−0·0000 (15)	−0·0029 (34)	−0·0044 (11)	−0·0024 (22)	−0·0025 (1)
4 0 0	−0·0022 (40)	0·0002 (110)	0·0035 (11)	0·0005 (29)	0·0003 (2)
3 3 0	−0·0084 (28)	−0·0108 (79)	−0·0043 (8)	−0·0078 (33)	−0·0079 (1)
4 1 1	0·0014 (19)	0·0025 (49)	0·0050 (7)	0·0030 (18)	0·0030 (1)
4 2 0	0·0057 (20)	0·0081 (63)	0·0102 (5)	0·0080 (23)	0·0080 (1)
3 3 2	−0·0037 (23)	−0·0030 (55)	−0·0075 (6)	−0·0047 (24)	−0·0048 (1)
4 2 2	−0·0051 (20)	−0·0015 (58)	−0·0057 (4)	−0·0041 (23)	−0·0041 (1)

$I_{SRO}(\mathbf{k})$ (●) is also shown. It can be seen that the diffuse X-ray intensity shows its maximum between the Bragg reflections indicating short-range ordering. The peak is slightly shifted from the $L1_2$-superstructure position demonstrating the influence of scattering contributions due to the static displacements. The separated short-range-order intensity contributes about 20% at maximum to the total diffuse intensity.

For the Williams analysis and the two separation methods data of the type × and ▲, respectively, were used. Whereas for the Georgopoulos–Cohen procedure the full range of scattering angles up to 90° was used, its range was reduced to less than 55° for the analysis with constant scattering-factor coefficients and for the direct least-squares fitting. This restriction was applied to reduce the influence of contributions due to displacement scattering and of any variation of the scattering-factor coefficients in **k** space. For the Williams analysis 29 parameters were determined (14 short-range-order parameters, seven first- and eight second-order displacement parameters). Because TDS can only be approximately calculated from elastic constants - which themselves show an uncertainty of 1–4% (Pottebohm, Neite & Nembach, 1983) - and because of its quadratic dependence on these constants, a multiplicative factor for TDS_1 was introduced as an additional fitting parameter. This parameter amounted to 1·05 and 1·22 for sample 1 and sample 2, respectively. For the separation methods, no restriction in the number of the structural parameters is necessary, and TDS_1 is included in the second-order displacement terms of (1).

A. Short-range order

The Warren–Cowley coefficients α_{lmn} for both crystals are given in Table 1. The errors of the solutions for the separation methods and for the Williams analysis were calculated after Wu, Matsubara & Cohen (1983) and from the covariance matrix, respectively. A second estimate of the error for each coefficient is given by the standard deviation of the mean values, obtained by arithmetically averaging over all three sets of short-range-order coefficients (column 4).

The value of α_{000}, which should be exactly unity, differs by nearly 20% from the theoretical value for sample 1. For sample 2, the deviation from unity (about 4%) is within the uncertainty of the calibration. This illustrates the improvement in data analysis obtained by the drastic reduction of background scattering by evacuating the sample surroundings.

The absolute values of α_{110} reach 84 and 90% of their maximum permitted value of $1 - c_{Ni}^{-1}$ for sample 1 and sample 2, respectively. This indicates a strong

ordering tendency. A preference for like second-nearest neighbours is expressed in positive values for the coefficients α_{200}. The small values for α_{211} reflect the very weak correlations for third-nearest neighbours.

The influence of counting statistics on the data analysis was studied by measuring sample 2 twice under identical conditions. These two complete data sets were then analysed identically after Georgopoulos & Cohen (1977) (in Table 1, the average values are given). The resulting differences of the Warren-Cowley parameters are more pronounced than fluctuations in these parameters due to uncertainties of experimental data such as the normalization factor, DWF *etc.*, but still smaller than the ones calculated after Wu, Matsubara & Cohen (1983). The observed standard deviations of the mean values, however, are of the same magnitude as the calculated errors. Therefore, these deviations from the mean values can be identified as the actual experimental errors.

For both samples the Warren-Cowley parameters α_{lmn} oscillate in the same way as in a fully ordered Ni_3Al crystal ($L1_2$ superstructure), as seen in Figs. 2(*a*) and (*b*). Short-range-order parameters higher than α_{422}, however, showed no significant deviation from $\alpha_{lmn}=0$, the value in a random solid solution.

The isointensity diagram for a (100) plane, reconstructed from the short-range-order parameters of the three different methods and from the averaged ones, is shown in Fig. 3 for sample 1. The agreement

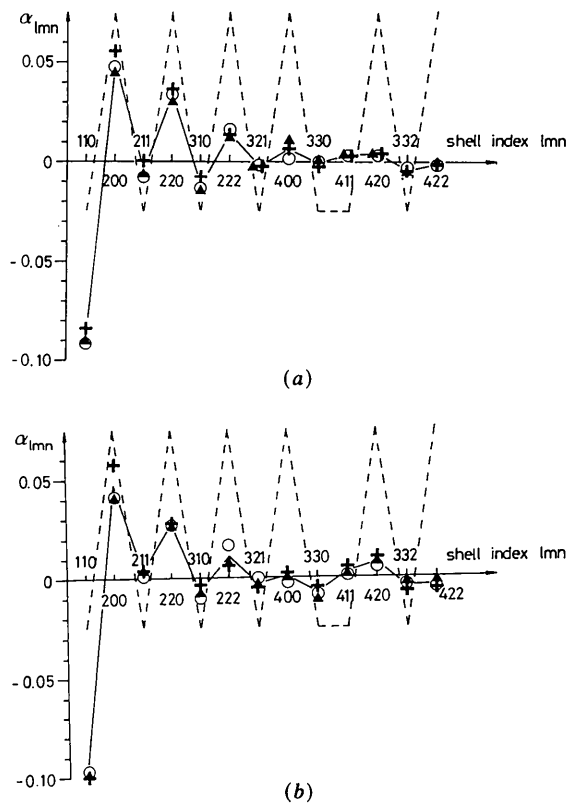

Fig. 2. Warren-Cowley short-range-order parameters α_{lmn} as a function of the coordination-shell index *lmn* for the $L1_2$ superstructure scaled by 0·075 (broken line) and for sample 1 (*a*) and sample 2 (*b*) with the evaluation methods of Georgopoulos & Cohen (○), of Borie & Sparks (▲) and of Williams (+).

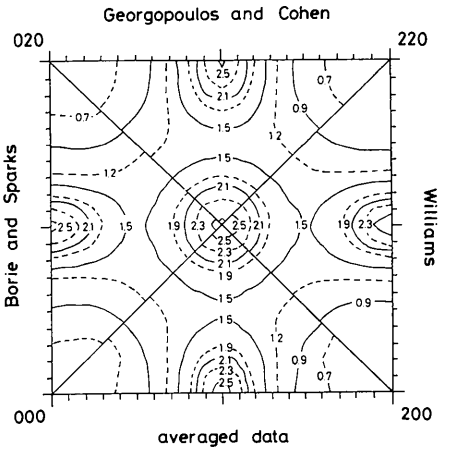

Fig. 3. Isointensity plot of $I_{SRO}(\mathbf{k})$ in Laue units for sample 1 reconstructed from the short-range-order parameters of the three methods and from the averaged ones.

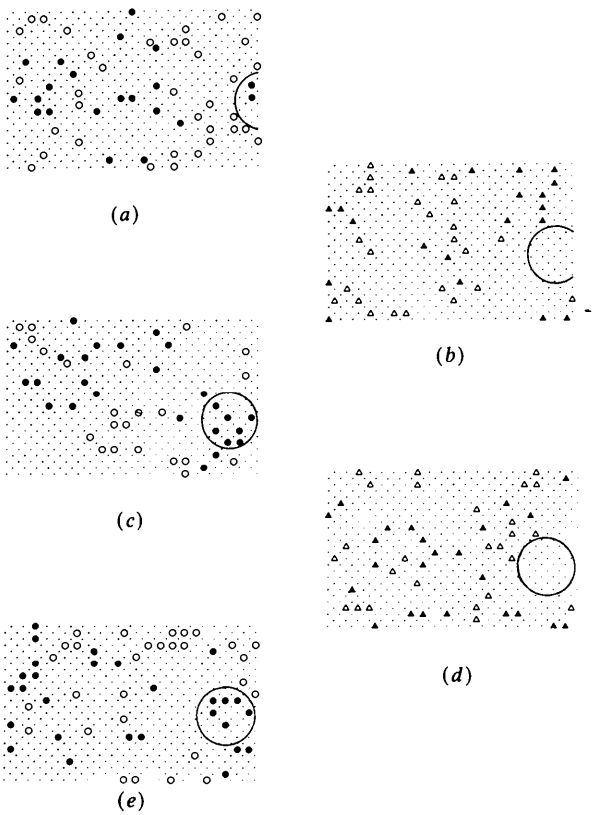

Fig. 4. (*a*) to (*e*) show consecutive (100) planes of the modelled sample 1 with ●, ○, ▲, △ representing Al atoms on the four sublattices and with • for any Ni atom.

Table 2. *Abundance analysis for the first coordination shell*

Sample 1

(i) Minority (Al) around majority (Ni) atoms

Configuration	Configuration abundance (%) Random	Quenched	Configuration	Configuration abundance (%) Random	Quenched
*C*1	30·18	19·98	*C*10	1·69	0·68
*C*2	37·97	43·79	*C*11	1·68	0·66
*C*3	4·09	9·00	*C*12	0·85	0·24
*C*4	1·97	4·67	*C*13	0·86	0·02
*C*5	8·06	13·36	*C*14	0·85	0·02
*C*6	7·85	1·93	*C*15	0·27	0·00
*C*7	0·42	2·15	*C*16	0·01	0·13
*C*8	0·85	2·43	*C*17	0·03	0·12
*C*9	0·28	0·55	*C*18	0·17	0·13
(ii) Minority (Al) around minority (Al) atoms					
C1	30·35	82·10	C4	1·77	0·18
C2	38·27	17·21	C5	7·63	0·30
C3	4·09	0·21	C6	8·30	0·00

Sample 2

(i) Minority (Al) around majority (Ni) atoms

*C*1	29·01	17·75	*C*10	1·77	0·45
*C*2	37·81	43·58	*C*11	1·76	0·50
*C*3	4·13	9·40	*C*12	0·94	0·19
*C*4	2·10	4·92	*C*13	0·91	0·01
*C*5	8·36	15·37	*C*14	0·85	0·00
*C*6	8·04	1·32	*C*15	0·27	0·00
*C*7	0·41	2·20	*C*16	0·01	0·12
*C*8	0·92	3·01	*C*17	0·04	0·12
*C*9	0·31	0·87	*C*18	0·18	0·07
(ii) Minority (Al) around minority (Al) atoms					
*C*1	28·56	87·89	*C*4	1·72	0·03
*C*2	37·37	11·94	*C*5	7·70	0·06
*C*3	4·14	0·06	*C*6	8·85	0·03

between any of the individual intensities I_x and I_y, defined by the ratio $[\sum (I_x - I_y)^2 / I_y^2]^{1/2}$, is better than 6% for sample 1 and 10% for sample 2. The agreement between the reconstructed intensities of the individual methods and the mean solution is better than 4% for sample 1 and 8% for sample 2. The agreement is worst between the separation methods and the Williams analysis. All three methods, however, characterize the short-range-order nature rather similarly, as can be seen in Figs. 2 and 3.

B. Crystal modelling

A more detailed picture of the local order is obtained by a computer simulation as first demonstrated by Gehlen & Cohen (1965). In this simulation, *A* and *B* atoms of a computer crystal (with the same composition as the crystal studied) are interchanged without any energy considerations. An interchange is only permitted if it improves the agreement with the experimental short-range-order parameters. In the present study the first 13 averaged Warren-Cowley coefficients of Table 1 were used to construct a computer crystal corresponding to these coefficients; the evaluation was based on a program of Williams (1976). The model crystal contained 13 104 atoms and was sufficiently large for the observed correlations. 900 (sample 1) and 1030 (sample 2) interchanges were performed to fit the experimental α_{lmn} within 2×10^{-4}. The resulting modelled parameters are listed in column 5 of Table 1. As an illustration, five consecutive (100) planes of the computer crystal are shown in Fig. 4 for sample 1. Again, the corresponding plot for sample 2 shows no significant differences. The positions of Al atoms on the four different sublattices of the f.c.c. lattice are labelled with different symbols; the lattice positions occupied by an Ni atom are always marked with a dot. In spite of the strong ordering tendency expressed by the large negative value of α_{110}, no indications of fully ordered particle-like regions were found. The encircled volume in Fig. 4, however, indicates an ordering of the Ni_3Al type.

A more detailed picture of the modelled structure is obtained by the inspection of the 144 distinguishable atomic configurations of the first coordination shell (Clapp, 1971). The results are presented in Table 2 for Ni or Al atoms as central atoms and compared with a modelled random array. The nomenclature used is illustrated in Fig. 5. It can be seen that over 99% of the atomic arrangements can be classified in one of the first 18 configurations. Compared with a random alloy the relative amount increases for those configurations where the Al atoms occupy only one f.c.c. sublattice as in the $L1_2$ superstructure, and

decreases for all configurations which include at least one Al–Al pair as nearest neighbours. The low abundance of the basic structure element of the Ni_3Al structure ($C16$) present in the short-range-ordered alloy, however, indicates that a model of dispersed perfectly ordered domains (Aubauer & Warlimont, 1974) is not appropriate to describe the present short-range-ordered structure. About one-sixth of all configurations are consistent with antiphase boundaries of the type (100), with the displacement vector within the boundary ($C5$, $C8$ and $C17$). Coordinated Al atoms thus occupy positions in more than one sublattice, but avoid forming Al–Al nearest-neighbour pairs.

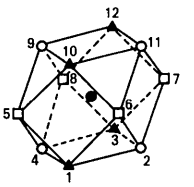

Configuration (Clapp, 1971)	Sites occupied by one specific type of atom
$C1$	—
× $C2$	6
× $C3$	6, 7
× $C4$	5, 7
$C5$	6, 12
× × $C6$	6, 11
× $C7$	5, 6, 7
$C8$	5, 6, 12
$C9$	1, 7, 9
× × $C10$	5, 6, 11
× × $C11$	4, 6, 11
× × $C12$	1, 5, 11
× × $C13$	2, 6, 11
× × $C14$	1, 6, 11
× × $C15$	6, 10, 11
× $C16$	5, 6, 7, 8
$C17$	4, 6, 7, 9
× × $C18$	5, 6, 8, 4

Fig. 5. Site numbering and nomenclature of configurations as introduced by Clapp (1971). ×: Configurations consistent with the $L1_2$ superstructure. ××: Configurations with at least one Al–Al pair as nearest neighbours.

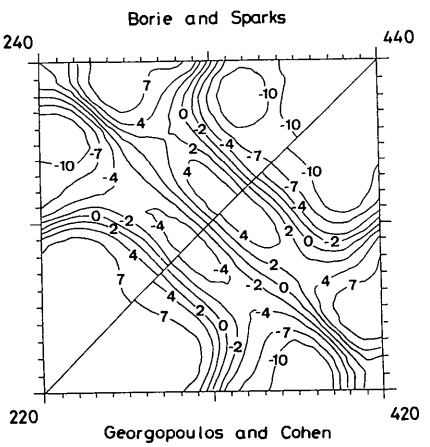

Fig. 6. Isointensity plot of the first-order displacement scattering in 0·1 Laue units for sample 1 with both separation methods.

Table 3. *First-order displacement parameters γ^x_{lmn} for the various evaluation methods*

Shell index *lmn*	Georgopoulos & Cohen (1977)	Borie & Sparks (1971)	Williams (1972)
Sample 1			
110/101	0·0454 (141)	0·0437 (10)	0·0471 (2)
200	−0·0339 (246)	−0·0384 (20)	−0·0330 (4)
211	−0·0104 (199)	−0·0094 (10)	−0·0061 (2)
112/121	0·0018 (78)	0·0026 (7)	0·0042 (2)
220/202	0·0215 (107)	0·0220 (10)	0·0247 (2)
310/301	−0·0104 (115)	−0·0077 (9)	−0·0009 (2)
103/130	−0·0013 (109)	−0·0008 (10)	0·0029 (2)
222	−0·0017 (118)	−0·0019 (9)	
321/312	0·0019 (78)	0·0026 (6)	
213/231	−0·0018 (75)	−0·0017 (7)	
132/123	0·0007 (80)	0·0009 (8)	
400	−0·0024 (255)	−0·0049 (21)	
330/303	0·0064 (118)	0·0067 (9)	
411	−0·0048 (105)	−0·0061 (9)	
114/141	−0·0014 (86)	−0·0034 (6)	
420/402	−0·0041 (109)	−0·0046 (11)	
204/240	−0·0020 (108)	−0·0038 (10)	
332/323	−0·0022 (77)	−0·0022 (7)	
233	−0·0001 (105)	−0·0013 (10)	
Sample 2			
110/101	0·0550 (113)	0·0532 (12)	0·0596 (3)
200	−0·0252 (237)	−0·0238 (23)	−0·0311 (6)
211	−0·0004 (103)	−0·0032 (11)	−0·0021 (3)
112/121	0·0080 (77)	0·0077 (8)	0·0078 (2)
220/202	0·0249 (114)	0·0212 (11)	0·0290 (3)
310/301	−0·0090 (122)	−0·0095 (11)	−0·0057 (3)
103/130	0·0015 (107)	−0·0039 (13)	0·0000 (3)
222	0·0020 (114)	0·0034 (10)	
321/312	0·0037 (73)	0·0028 (7)	
213/231	0·0004 (74)	−0·0007 (8)	
132/123	−0·0008 (77)	0·0000 (10)	
400	−0·0096 (236)	−0·0117 (23)	
330/303	0·0092 (115)	0·0082 (12)	
411	−0·0058 (103)	−0·0016 (11)	
114/141	−0·0028 (75)	−0·0031 (8)	
420/402	−0·0029 (104)	−0·0031 (13)	
204/240	−0·0028 (105)	0·0011 (12)	
332/323	−0·0010 (85)	0·0000 (8)	
233	0·0021 (107)	0·0034 (11)	

The analysis of the first coordination shell suggests an $L1_2$ type of ordering. This finding is further substantiated by the results for the octahedral second- and the cuboctahedral fourth-neighbour shells, where the central atom and the coordinated atoms belong to the same sublattice. If one starts with an Al atom as central atom, both coordination shells show a tendency for the sublattice defined by the central Al atom to be occupied by further Al atoms.

C. *Static atomic displacements*

The analysis according to Georgopoulos & Cohen (1977) allows one to determine the mean atomic displacements for both components separately. Although the errors are as large or even larger than the values obtained by Fourier inversion of equations like (6), it can be concluded that Ni–Ni pairs undergo lattice displacements of about 0·1% with respect to the mean lattice parameter, whereas the displacements between Al–Al pairs are larger, amounting to

about 4%. The mean lattice of the alloy is therefore mainly determined by the Ni atoms. Because of the large value of α_{110}, the determination of $\langle x_{lmn}^{\text{Al-Al}} \rangle$ is strongly influenced by the error of α_{110}, which prevents an interpretation of the Al-Al nearest-neighbour distance.

To compare the mutual agreement of the three methods in the evaluation of the first-order-displacement parameters, γ_{lmn}^{x} was calculated after (8) assuming constant (averaged) scattering-factor ratios $\langle \eta \rangle = -0{\cdot}7258$ and $\langle \xi \rangle = -1{\cdot}7258$. The values for γ_{lmn}^{x} are listed in Table 3 together with the Fourier coefficients γ_{lmn}^{x} of the Borie-Sparks and the Williams analyses. A good agreement of the corresponding parameters among themselves is found for both samples. In Fig. 6, the total first-order displacement intensity of sample 1, reconstructed from γ_{lmn}^{x} of the two separation methods, is plotted in a (100) plane around the 330 position. The asymmetry with respect to the 330 superstructure position, responsible for the shift of the diffuse intensity maximum (Fig. 1), is quite pronounced. The differences in the first-order-displacement intensities of the two samples are located near the Bragg positions, where sample 2 shows higher intensity values. This is just the region where $I_{\text{SRO}}(\mathbf{k})$ has to be extrapolated in order to obtain the minimum separation volume.

5. Discussion

If one compares sample 1 and sample 2, the largest differences in the diffuse scattering intensities are found close to the Bragg reflections and in the coefficients α_{000}. Though the latter difference can be explained by the reduction of air scattering, the differences in the multiplicative factor of TDS_1 indicate still other unseparated intensities. Excess intensities in the tails of Bragg reflections seem to be decisive.

In Fig. 3 the ellipsoidal shape of the diffuse short-range-order maximum is striking. Similar effects were observed in Cu_3Au (Bardhan & Cohen, 1976), Cu_3Pd (Ohshima, Watanabe & Harada, 1976) and in Ni-23·5 at.% Fe (Lefebvre, Bley, Bessière, Fayard, Roth & Cohen, 1980). The latter authors related this shape to the unexpectedly small value of α_{211}. As seen in Fig. 2, this value is also small in the present study. It is not clear whether this behaviour is related to antiphase boundaries on {100} planes or to the plate-like nature of the ordered regions. The results of the computer modelling, however, are more compatible with the latter feature (see Fig. 4).

The first-order-displacement parameters from both samples are of the same order of magnitude as the coefficients of Cu_3Au (Bardhan & Cohen, 1976), Cu_3Pd (Ohshima, Watanabe & Harada, 1976) and Au_3Cu (Bessière, Lefebvre & Calvayrac, 1983). In agreement with the sign of the size effect, the sign of the displacement parameters γ_{lmn}^{x} of Cu_3Au and Cu_3Pd show the same and those of Au_3Cu show an inverse sign sequence in comparison with the first few γ_{lmn}^{x} of the Ni-Al crystals studied here.

In the present investigation of a quenched-in state of short-range order three evaluation methods have been compared successfully for the first time. Lefebvre, Bley, Fayard & Roth (1981) analysed diffuse neutron scattering data of Fe_3Al after the Borie-Sparks procedure using the separation according to Gragg & Cohen (1971), and also with the Williams method. For both methods, a good agreement was found for the short-range-order parameters. It was concluded that the less laborious Williams method will produce reliable results for neutron scattering data if the displacements are sufficiently small. A test of all three methods was tried by Georgopoulos & Cohen (1981) who evaluated the diffuse X-ray scattering from non-stoichiometric β'-NiAl. It was found that in their case neither the separation procedure with constant scattering-factor ratios nor the Williams method gave acceptable solutions. In the present case, meaningful solutions for the Warren-Cowley parameters α_{lmn} and also for the first-order displacement coefficients γ_{lmn}^{x} were obtained with all three methods, although the first-order displacement parameters are of the same order as for β'-NiAl. Thus, more alloy systems must be studied in sufficient detail before a criterion for the validity of the various evaluation procedures can be established.

The authors are grateful to Professors J. B. Cohen and P. Georgopoulos (Northwestern University, Evanston), who kindly made available their data analysis package. They wish to thank E. Fischer for growing the single crystal used in the experiment and A. Blanchard for drawing the figures. This paper represents part of a thesis submitted by FK in partial fulfilment of the requirements for a Dr Sci. Nat. degree at the ETH Zürich. Financial support of the project 'Microstructure and Mechanical Properties of Superalloys' by the Nationaler Energieforschungsfonds (NEFF) and the Schweizerischer Nationalfonds is gratefully acknowledged.

References

AUBAUER, H. & WARLIMONT, H. (1974). *Z. Metallkd.* **65**, 297-303.
BARDHAN, P. & COHEN, J. B. (1976). *Acta Cryst.* A**32**, 597-614.
BATTERMAN, B. W., CHIPMAN, D. R. & DE MARCO, J. J. (1961). *Phys. Rev.* **122**, 68-74.
BEDDOE, R. E., HAASEN, P. & KOSTORZ, G. (1984). In *Decomposition of Alloys: the Early Stages*, edited by P. HAASEN, V. GEROLD, R. WAGNER & M. F. ASHBY, pp. 233-238. Oxford: Pergamon Press.
BESSIÈRE, M., LEFEBVRE, S. & CALVAYRAC, Y. (1983). *Acta Cryst.* B**39**, 145-153.
BORIE, B. & SPARKS, C. J. (1971). *Acta Cryst.* A**27**, 198-201.
CLAPP, P. C. (1971). *Phys. Rev. B*, **4**, 255-270.
COWLEY, J. M. (1950). *J. Appl. Phys.* **21**, 24-30.

CROMER, D. T. (1969). *J. Chem. Phys.* **50**, 4857-4859.
CROMER, D. T. & LIBERMAN, D. (1970). *J. Chem. Phys.* **53**, 1891-1898.
DOYLE, P. A. & TURNER, P. S. (1968). *Acta Cryst.* A**24**, 390-397.
EPPERSON, J. E. & FÜRNROHR, P. (1983). *Acta Cryst.* A**39**, 740-746.
GEHLEN, P. C. & COHEN, J. B. (1965). *Phys. Rev. A*, **139**, 844-855.
GEORGOPOULOS, P. & COHEN, J. B. (1977). *J. Phys.* **12**, C7, 191-196.
GEORGOPOULOS, P. & COHEN, J. B. (1981). *Acta Metall.* **29**, 1535-1551.
GRAGG, J. E. & COHEN, J. B. (1971). *Acta Metall.* **19**, 507-519.
GRÖHLICH, M., HAASEN, P. & FROMMEYER, G. (1982). *Scr. Metall.* **16**, 367-370.
KOSTORZ, G. (1983). In *Physical Metallurgy*, 3rd ed., edited by R. W. CAHN & P. HAASEN, pp. 793-853. New York: North-Holland.
LEFEBVRE, S., BLEY, F., BESSIÈRE, M., FAYARD, M., ROTH, M. & COHEN, J. B. (1980). *Acta Cryst.* A**36**, 1-7.
LEFEBVRE, S., BLEY, F., FAYARD, M. & ROTH, M. (1981). *Acta Metall.* **29**, 749-761.
LE PAGE, Y., GABE, E. J. & CALVERT, L. D. (1979). *J. Appl. Cryst.* **12**, 25-26.
MATSUBARA, E. & COHEN, J. B. (1983). *Acta Metall.* **31**, 2129-2135.
OHSHIMA, K.-I., WATANABE, D. & HARADA, J. (1976). *Acta Cryst.* A**32**, 883-892.
POTTEBOHM, H., NEITE, G. & NEMBACH, E. (1983). *Mater. Sci. Eng.* **60**, 189-194.
SCHWARTZ, L. H. & COHEN, J. B. (1977). *Diffraction from Materials.* New York: Academic Press.
SPARKS, C. J. & BORIE, B. (1965). In *Local Atomic Arrangements Studied by X-ray Diffraction*, edited by J. B. COHEN & J. E. HILLIARD, pp. 3-50. New York: Gordon & Breach.
WARREN, B. E. (1969). *X-ray Diffraction.* Reading, MA: Addison-Wesley.
WENDT, H. & HAASEN, P. (1983). *Acta Metall.* **31**, 1649-1659.
WILLIAMS, R. O. (1972). *A Computer Program for the Reduction of Diffuse X-ray Data from Solid Solutions.* Report ORNL-4828. Oak Ridge National Laboratory, Oak Ridge, Tennessee, USA.
WILLIAMS, R. O. (1976). *A Computer Program for the Simulation of Solid Solutions.* Report ORNL-5140. Oak Ridge National Laboratory, Oak Ridge, Tennessee, USA.
WU, T. B., MATSUBARA, E. & COHEN, J. B. (1983). *J. Appl. Cryst.* **16**, 407-414.

Acta Cryst. (1987). A**43**, 533-539

Difference Fourier Syntheses in Fiber Diffraction

BY KEIICHI NAMBA* AND GERALD STUBBS

Department of Molecular Biology, Vanderbilt University, Nashville, TN 37235, *USA*

(*Received* 8 *September* 1986; *accepted* 13 *January* 1987)

Abstract

Theory applying to difference Fourier syntheses from fiber diffraction data is developed, including the calculation of expected peak heights and noise levels. The signal-to-noise ratio in fiber diffraction difference maps is much lower than in crystallography, because of the multi-dimensional nature of fiber diffraction data, but it is shown by means of examples from tobacco mosaic virus that high-order difference syntheses, for example using coefficients analogous to crystallographic $6F_{obs}-5F_{calc}$, can clearly reveal differences between an observed structure and a model. 'Omit' maps, calculated from models by omitting a region under particular scrutiny, are of limited use in fiber diffraction, but maps calculated from hybrid coefficients derived from both full and partial models have some applications.

Introduction

Difference syntheses have been widely used in both protein and small-molecule crystallography to determine structures related to already known structures, and as part of refinement procedures (Blundell & Johnson, 1976; Glusker & Trueblood, 1985). Although they have found some use in fiber diffraction [a number of references are given by Mandelkow, Stubbs & Warren (1981)], this use has until now been limited by the difficulties peculiar to fiber diffraction which arise from the cylindrical averaging of fiber diffraction patterns. Difference Fourier maps calculated from fiber diffraction data by direct analogy with crystallographic difference maps tend to have high noise levels and to be biased toward the known or model structure, as will be shown below. In favorable cases, modification of the model structure has enabled interpretable maps to be calculated (Mandelkow, Stubbs & Warren, 1981), but no systematic procedure has been available to deal with the general case.

In this paper, we develop the theory of fiber diffraction difference Fourier syntheses, and illustrate the method with examples that use simulated data sets, calculated from an atomic model of tobacco mosaic virus (TMV). We also present several alternative, semi-empirical syntheses, that have proven effective in handling real data.

* Present address: ERATO, 5-9-5 Tokodai, Toyosato, Tsukuba 300-26, Japan.

0108-7673/87/040533-07$01.50